This is a repository copy of *Realization of the welding of individual TiO2 semiconductor nano-objects using a novel 1D Au80Sn20 nanosolder*.

White Rose Research Online URL for this paper:
http://eprints.whiterose.ac.uk/93841/

Version: Accepted Version

Article:

Qu, K., Zhang, H., Lan, Q. et al. (8 more authors) (2015) Realization of the welding of individual TiO2 semiconductor nano-objects using a novel 1D Au80Sn20 nanosolder. Journal of Materials Chemistry C, 3 (43). pp. 11311-11317. ISSN 2050-7526

https://doi.org/10.1039/c5tc01267h

Reuse
Unless indicated otherwise, fulltext items are protected by copyright with all rights reserved. The copyright exception in section 29 of the Copyright, Designs and Patents Act 1988 allows the making of a single copy solely for the purpose of non-commercial research or private study within the limits of fair dealing. The publisher or other rights-holder may allow further reproduction and re-use of this version - refer to the White Rose Research Online record for this item. Where records identify the publisher as the copyright holder, users can verify any specific terms of use on the publisher's website.

Takedown
If you consider content in White Rose Research Online to be in breach of UK law, please notify us by emailing eprints@whiterose.ac.uk including the URL of the record and the reason for the withdrawal request.

eprints@whiterose.ac.uk
https://eprints.whiterose.ac.uk/

Journal of
Materials Chemistry C

Accepted Manuscript

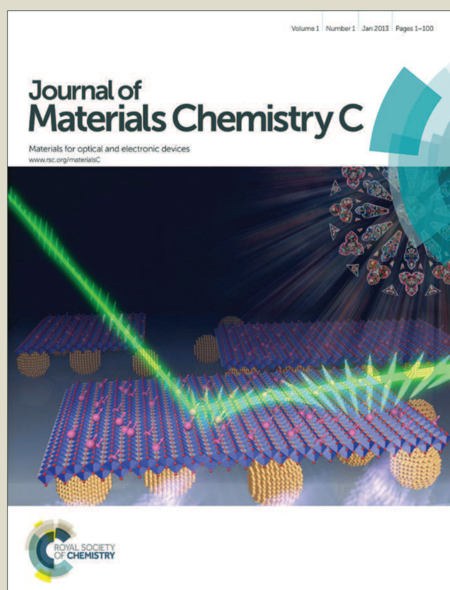

This is an *Accepted Manuscript*, which has been through the Royal Society of Chemistry peer review process and has been accepted for publication.

Accepted Manuscripts are published online shortly after acceptance, before technical editing, formatting and proof reading. Using this free service, authors can make their results available to the community, in citable form, before we publish the edited article. We will replace this *Accepted Manuscript* with the edited and formatted *Advance Article* as soon as it is available.

You can find more information about *Accepted Manuscripts* in the Information for Authors.

Please note that technical editing may introduce minor changes to the text and/or graphics, which may alter content. The journal's standard Terms & Conditions and the Ethical guidelines still apply. In no event shall the Royal Society of Chemistry be held responsible for any errors or omissions in this *Accepted Manuscript* or any consequences arising from the use of any information it contains.

ROYAL SOCIETY OF CHEMISTRY

www.rsc.org/materialsC

Journal Name

ARTICLE

Realization of the Welding of Individual TiO_2 Semiconductor Nanoobjects by Using Novel 1D $Au_{80}Sn_{20}$ Nanosolder

Received 00th January 20xx,
Accepted 00th January 20xx

DOI: 10.1039/x0xx00000x

www.rsc.org/

Ke Qu,[a] Hong Zhang,[a] Qianqian Lan,[a] Xia Deng,[a] Xinlong Ma,[a] Yuanqing Huang,[a] Junwei Zhang,[a] Hongbin Ma,[a] Beverley J Inkson,[b] Desheng Xue[a] and Yong Peng*[a]

Individual semiconductor nanowires (NWs) TiO_2 were successfully welded together by using novel one-dimensional (1D) $Au_{80}Sn_{20}$ (mass ratio) nanosolders at the nano scale for the first time. The nanosolders were electrodeposited into nanoporous templates to form 1D structure, and their morphology, crystal structure, chemistry and elemental electronic states were systematically characterized. Individual $Au_{80}Sn_{20}$ nanowires were proved to consist of mixed crystal phases, including Au5Sn phase with trigonal structure, AuSn phase with hexagonal structure and little SnO_2 phase produced by oxidation of the surface portion. Chemical analysis indicates that the composition is $Au_{80}Sn_{20}$. The testing of welding capability either in situ TEM or in situ SEM by nanomanipulators and Infiltration experiment reveal a good wet ability and diffusion ability between the $Au_{80}Sn_{20}$ nanosolder and TiO_2 nanowire. It is believed that our work contribute a special nanosolders for future nanoscale welding techniques, which also make the bondings of titanium-based semiconductor oxide nanomateirals at the nanoscale a reality.

1. INTRODUCTION

Welding techniques at the nano scale is crucial to the development of nanoscience and nanotechnology because the full utilization of the novel physical and chemical properties of individual nanoobjects is requested to bond them together into nano-electronics, nano-sensors and nano-devices.[1-3] Several nanowelding techniques, including thermal heating[4] , ion beam deposition[5, 6] , laser heating[7] , ultrasonic welding[8] , electrical welding technique[9] , high-energy electron beam irradiation[10] , and Joule heating[11-13] , has been invented to joint nanoparticles, nanowires, nanobelts, or nanotubes together at the nanoscale so far. For example, the electrical welding technique was used to weld individual Au NWs into nanocircuits and nanopatterns[9] . The high-energy electron beam irradiation (EBI) welding technique was used to bond carbon nanotubes together,[14] or metallic NWs (Au, Ag, Ni) with a Si NW which forms metal-semiconductor nanojoints.[10] However, current nanowelding body materials are dominated to be metallic nanowires and carbon nanotubes. The welding of semiconductor oxide nanoobjects is surprisedly sparse.

Semiconductor oxide nanomaterials have many novel and unique electrical, optical, chemical and biological properties,[15] which lead to a great interest for their usage in the fabrication of the next generation nanocircuits, nanotools, nanowires lasers, photon tunneling devices, near-field photo-waveguide devices, etc.[16] Titanium dioxide (TiO_2) NWs as one member of the semiconductor oxide nanomaterial family are considered to have a wide application into photoelectric conversion and energy saving fields based on their optical, photocatalytic, photohydrophilic properties.[17, 18] Bonding individual TiO_2 nano-objects together or with electrode pads to form secure, functional and long-lasting nanoscale systems is significant and urgent for the quick realisation of their practical applications. There are two attempts on the welding of TiO_2 NWs onto electrode pads.[19, 20] But, individual TiO_2 NWs have not been welded together so far as far as we know. It is believed to be due to the high melting point and good chemical stability of TiO_2, which is not conductive to bond them together directly. Alike traditional welding method, using a proper solder media to bond the TiO_2 nanoobjects should be an effective way, which also have the opportunity to specifically tailor the weld properties of these joints such as chemistry, strength, and conductivity.

Many studies have shown that there exists good diffusion between titanium and gold.[21, 22] In the previous report,[22] Ti was verified to sufficiently diffuse through 260 nm Au thin film at temperatures ranging between 200 and 400 ℃, and the surfacial oxidation of Ti can enhance the diffusion. Therefore, it is feasible to utilize gold-rich nanosolders with a moderate melting point to weld titanium-based semiconductor nanometarils at the nano scale. It is worthy to note that the electronic industry banned the lead to use as an elemental composition of solders on 1 July 2006 due to its high toxicity and environmental pollution. The exploitation and studies of Au-Sn solders become more important and necessary, especially, when the nanoscale welding techniques have turned into practical ways to connect nanoscale building

a. *Key Laboratory of Magnetism and Magnetic Materials of the Ministry of Education, Lanzhou University, Lanzhou 730000, P. R. China. E-mail: pengy@lzu.edu.cn; Fax: +86 931 8914160; Tel: +86 931 8912425*
b. *Department of Materials Science and Engineering, Sheffield S1 3JD, UK*
† Electronic Supplementary Information (ESI) available: additional curve, TEM image and HADDF-STEM image. See DOI: 10.1039/x0xx00000x

Journal of Materials Chemistry C Accepted Manuscript

blocks in the future nano industry. $Au_{80}Sn_{20}$ alloy solder composed of 80 wt% gold and 20 wt% tin could be a good candidate, which is at the eutectic point with a relatively low melting point of 278 ℃ on Au-Sn binary phase diagram. As an important industrial solder, $Au_{80}Sn_{20}$ solder is typically used in the welding of opto/microelectronic packaging areas,[23] and semiconductor materials. In comparison with the conventional solders, $Au_{80}Sn_{20}$ solder has many excellent properties, such as high strength, good corrosion resistance, high thermal conductivity, good electrical properties, free-flux, and so on, which make it an ideal solder.[24-27] However, nanoscale $Au_{80}Sn_{20}$ alloy and its application into individual nanoscale building blocks of semiconductor or other materials in nano space have not been reported so far.

In this work, we present a preparation of 1D $Au_{80}Sn_{20}$ alloy nanosolders by using electrodeposition into nanoporous templates. The morphological, structural and chemical characterizations of 1D $Au_{80}Sn_{20}$ alloy nanosolders have been systemically investigated. Furthermore, the $Au_{80}Sn_{20}$ nanosolders have been used to weld individual TiO_2 NWs together. It is believed that our work not only contributes an important nanosolder for the nanowelding techniques, but also takes the first step to realize the welding of semiconductor oxide nanomaterials, which is critical and significant for the transformation of semiconductor nanomaterials into nano-electronics, nano-sensors or nano-devices.

2. EXPERIMENTAL SECTION

2.1. Preparation of 1D $Au_{80}Sn_{20}$ alloy nanosolders.

1D $Au_{80}Sn_{20}$ alloy nanosolders were prepared by DC electrodeposition into anodic aluminum oxide (AAO) templates or polycarbonate (PC, Anodisc, Whatman Inc., Florham Park, NJ, USA) templates with 50 nm diameter pores. The AAO templates were prepared in-house, of which detailed procedures were described in our previous report.[28, 29] One side of the non-barrier-layered AAO/PC templates was sputtered by thermally evaporating a 50 nm Ag thin film, serving as the working electrode. The electrodeposition was achieved in a three-electrode electrolytic cell at room temperature on a CHI630B electrochemical workstation, in which the reference electrode was a saturated calomel electrode (SCE) and the counter-electrode was a graphite sheet. The electrodeposition electrolyte is composed of 0.016 M $HAuCl_4{\bullet}4H_2O$, 0.007 M $SnCl_2{\bullet}2H_2O$, 0.125 M ammonium citrate, 0.059 M Na_2SO_3 and 0.01 M L-ascorbic acid. $HAuCl_4{\bullet}4H_2O$ and $SnCl_2{\bullet}2H_2O$ are the main salts to provide Au^{3+} and Sn^{2+}. Na_2SO_3 is a complexing agent for Au^{3+}. Ammonium citrate is a complexing agent for Sn^{2+}, and also an auxiliary complexing agent for Au^{3+}. L-ascorbic acid is an antioxidant. The pH value of the electrodeposition electrolyte was 5.5-6.0. Voltammetric experiments were completed to determine the optimal electrodeposition potentials for the co-electrodeposition AuSn alloy. In this work, a -1.4 V potential is applied to obtain $Au_{80}Sn_{20}$ eutectic alloy nanosolders, of which typical curve of the time dependence of the observed current during the growth of AuSn alloy nanowires in AAO/PC templates is shown in Fig. S1. The chemical composition of AuSn alloy nanosolders is strongly dependent on electrodeposition potential. According to XPS analysis, a -1.3 V potential obtained a $Au_{50}Sn_{50}$ composition. The typical deposition time for PC templates is set up to 30 mins, and for AAO templates is 120 mins, which determine the length of nanowires (Fig. S2). The electrodeposition electrolyte was continuously agitated throughout by a magnetic stirrer.

2.2. Fabrication of TiO_2 nanowires.

TiO_2 nanofibers were fabricated by using a conventional electrospinning method. In a typical synthesis, 1.2 ml tetrabutyl titanate was mixed with 2.2 ml acetic acid and 1.6 ml ethanol. After 10 min, 3.6 ml ethanol and 0.4 g PVP (Aldrich, Mw ≈ 1 300 000) were added, followed by magnetic stirring for about 1 h (with the solution held in a capped bottle). The mixture was immediately loaded into a plastic syringe equipped for electrospinning. The electrospinning process was performed by a dedicated electrospinning facility at 18 kV DC voltage, 15 cm spacing between needle tip and collector, and a feed rate was fixed with 0.4 ml/h. The electrospun polymer composite fibers were collected using alumina crucibles and then calcined at 500 ℃ for 2 h with a heating rate of 1 ℃/min in air. The sample was finally allowed to cool to room temperature.

2.3. Characterization.

The morphological, crystal structural and chemical characterisation of the 1D $Au_{80}Sn_{20}$ nanosolder were analyzed on a nano-scale using field emission scanning electron microscopy (FESEM, Tescan Mira 3 xmu, Czech Republic), high-resolution transmission electron microscope (HRTEM, TecnaiTM G2 F30, FEI, US) equipped with energy-dispersive X-Ray analysis (EDAX, AMETEK Co., LTD), high angle annular dark field and scanning transmission electron microscopy (HAADF-STEM), X-ray photoelectron spectroscopy (XPS, Kratos Axis Ultra DLD, Japan). The AAO templates or PC templates were completely dissolved in 0.1 M sodium hydroxide solution or dichloromethane for releasing nanowires, which are then rinsed with distilled water and dispersed on holey carbon coated copper grids for TEM, STEM, EDX and analysis.

2.4. Welding of TiO_2 nanowires in situ TEM and in situ SEM by nanomanipulators.

The testing of welding capability of 1D $Au_{80}Sn_{20}$ nanosolder into TiO_2 semiconductor oxide nanowires at the nanoscale space were carried out in-situ the HRTEM operated at 300 kV and spot size 1. Individual TiO_2 nanowires and $Au_{80}Sn_{20}$ nanosolders were successively dispersed on holey carbon coated Cu grids to obtain cross-sectioned structures.

A similar quality test was also carried out by using four nanomanipulators (Kleindiek Nanotechnik, Germany) equipped with nichrome nanotips and a Keithley 6487 picoammeter in situ SEM to weld TiO_2 nanopatterns at the

Journal of Materials Chemistry C Accepted Manuscript

This journal is © The Royal Society of Chemistry 20xx

nanoscale. The data acquisition and nanowelding signal were automated using a dedicated multifunctional program.

2.5. Infiltration experiment.

The nanowire solder infiltration experiments were carried out in a programmable high-temperature tube furnace. The solder nanowires were dropped onto TiO_2 substrate and SiO_2 substrate. TiO_2 substrate was fabricated by a spin-coating method[30] and SiO_2 substrate was obtained commercially. Nitrogen purging was used to avoid a further oxidation of nanosolders during this process. The temperature was firstly increased to approximate 200 ℃ ~ 220 ℃ for 5 min to preheat the wires, then briefly raised to 320 ℃ for 30 min to ensure a complete melt and diffusion. The TiO_2/SiO_2 substrates were cooled down to room temperature and then brought out of the furnace. The detection of infiltration effect was assisted by two in situ SEM nanomanipulators (Kleindiek Nanotechnik, Germany) equipped with nichrome nanoprobes/nanotips.

3. Results and Discussion

3.1. Morphologies, crystal structural and chemical characterization of individual 1D $Au_{80}Sn_{20}$ nanosolders.

Fig. 1a shows a representative HAADF-STEM image of a bundle of 1D $Au_{80}Sn_{20}$ nanosolders prepared by polycarbonate (PC) template, of which PC template has been completely dissolved. Individual $Au_{80}Sn_{20}$ nanowires have uneven diameter, alike cylinders, which are replica of the channels of PC templates. The size statistics reveals that the top diameter is approximately 50 nm and the bottom diameter is approximately 120 nm. The average length for the most of nanowires is around 3 µm. The 1D $Au_{80}Sn_{20}$ nanowires prepared by AAO template are seen in Fig. 1b, showing a continuous structure with uniform size and large aspect ratio, alike hairs. The size statistics reveals that the average diameter of the prepared $Au_{80}Sn_{20}$ nanowires is approximately 50 nm. The average length for the most of nanowires is about 5 µm.

The crystalline structures of individual 1D $Au_{80}Sn_{20}$ nanosolders are characterized in detail using selected-area electron diffraction (SAED) and high-resolution TEM (HRTEM). The large magnified TEM image as shown in Fig. 1c displays that individual $Au_{80}Sn_{20}$ nanowires consist of many crystal grains stacking along the nanowire axis, and the surface is slightly oxidized (about 3~4 nm thickness, as marked by red double lines). Its corresponding SAED pattern is shown in Fig. 1d, revealing that the individual 1D $Au_{80}Sn_{20}$ nanosolders is multi-crystal. The rings can be well indexed to two sets of lattice planes. The yellow one can be well indexed to the (110), (006), (116), (300) and (223) planes of the trigonal Au5Sn phase. The red one can be well indexed to the (102), (210), (212), (114) and (205) planes of the hexagonal AuSn phase. Fig. 1e and 1f show lattice-resolution images of the Au5Sn phase and AuSn phase marked by white squares E and F in Fig. 1c. The interplanar distances are measured to be 2.247 Å and 2.546 Å for Au5Sn phase in Fig. 1e, matching with (113) and (110) planes of the trigonal Au5Sn phase. The interplanar distances are measured to be 1.773 Å and 2.222 Å for AuSn phase in Fig. 1f, matching with (201) and (102) planes of the hexagonal AuSn phase. The corresponding FFT patterns and crystal structure simulation of the areas 'E' and 'F' are shown in the insets of Fig. 1e and 1f. The crystal structure was further investigated by XRD technique. Figure S3 shows a typical XRD spectrum of 1D $Au_{80}Sn_{20}$ nanosolders embedded into PC templates with a 100 nm Cu thin film evaporated as the working electrode, which also shows a mixture of trigonal Au5Sn crystal phase and hexagonal AuSn crystal phase. It is then concluded that the as-deposited 1D $Au_{80}Sn_{20}$ nanosolder is comprised of trigonal Au5Sn phase and hexagonal AuSn phase, which preserve their bulk crystal structure.[24]

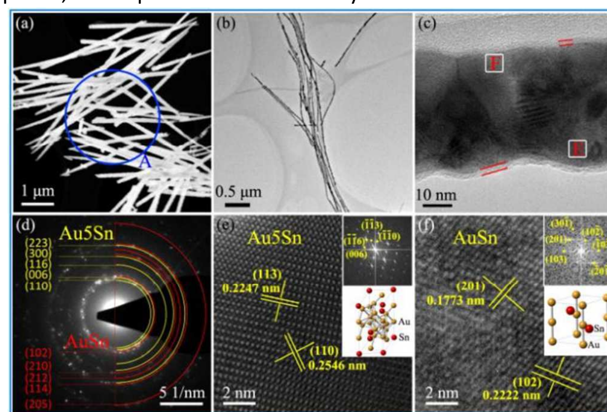

Fig. 1. (a) HAADF-STEM image of 1D $Au_{80}Sn_{20}$ nanosolders dissolved from PC template. (b) TEM image of single 1D $Au_{80}Sn_{20}$ nanosolder fabricated by AAO template. (c) The large magnified TEM image of individual 1D $Au_{80}Sn_{20}$ nanosolders. (d) SEAD image of individual 1D $Au_{80}Sn_{20}$ nanosolders. Yellow for Au5Sn phase and red for AuSn phase. (e) and (f) Lattice-resolution HRTEM image of Au5Sn phase and AuSn phase form the white squares in (c). Insets, the corresponding FFT patterns and crystal structure simulation.

The chemical composition of individual $Au_{80}Sn_{20}$ alloy nanosolder is analyzed by EDX spectrum (in Fig. 2a), of which detected area come from the region A marked by blue circle in Fig. 1a. The Au and Sn peaks come from the 1D $Au_{80}Sn_{20}$ alloy nanosolders. The O peak originates from the thin oxide layer covered on the surfaces of the 1D nanosolders as observed in Fig. 1c, which is deduced to their exposure in the air after released from the templates. The C and Cu peaks are believed to derive from the holey carbon coated copper grid, which was confirmed by the measurement of an EDX baseline of an empty holey carbon coated copper grid. Quantitative analysis of this spectrum reveals that the chemical composition of individual 1D $Au_{80}Sn_{20}$ nanosolders is a 80.1:19.9 weight ratio of Au:Sn, referring a $Au_{80}Sn_{20}$ chemical phase. The chemical elemental distributions of 1D $Au_{80}Sn_{20}$ nanosolders were further studied by EDX elemental mapping analysis techniques (Fig. 2b-d). Fig. 2b shows a representative HADDF-STEM image of two 1D $Au_{80}Sn_{20}$ nanosolders. Fig. 2c and 2d display the EDX elemental mappings of Au-Lα (9.71 keV) and Sn-Lα (3.44 keV), respectively. The elements of Au and Sn are evenly distributed

Journal of Materials Chemistry C Accepted Manuscript

Please do not adjust margins

throughout the whole nanosolder, indicating a uniform $Au_{80}Sn_{20}$ chemical phase.

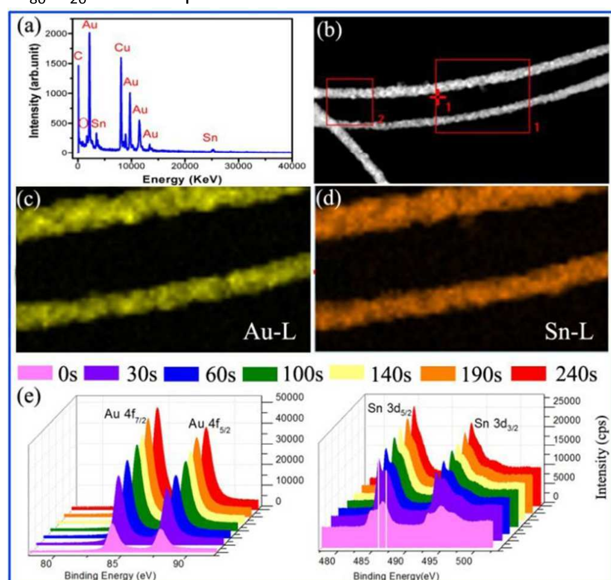

Fig. 2. Chemical analysis of the 1D $Au_{80}Sn_{20}$ nanosolders: (a) EDX spectrum of a bundle of 1D $Au_{80}Sn_{20}$ nanosolders from Fig. 1a as marked by blue circle. (b) HAADF-STEM image. (c) Au elemental mapping. (d) Sn elemental mapping. (e) XPS spectra of Au 4f and Sn 3d after the specimen was sputtered by Ar ion for 0, 30, 60, 100, 140, 190 and 240 s, respectively. Pink for 0 s, purple for 30 s, blue for 60 s, green for 100 s, yellow for 140 s, orange for 190 s, red for 240 s.

In order to accurately determine the electronic states, the as-grown 1D $Au_{80}Sn_{20}$ nanosolders were further examined by XPS while they were still in situ embedded in the PC templates. The Ar ion beam sputtering was employed to realize the analysis of layer by layer. The templates were cross-sectioned from the top surface of the PC template, which was parallel to the 1D $Au_{80}Sn_{20}$ nanosolder length axes. Fig. 2e shows the relevant XPS spectra of Au 4f and Sn 3d after Ar ion beam sputtering for 0 s, 30 s, 60 s, 100 s, 140 s, 190 s and 240 s, respectively. The binding energies were calibrated by using the C 1s peak of 285 eV as a standard. It is seen that the Au 4f 7/2 peaking at 84.0 eV bonding energy in Fig. 2e can be attributed to AuSn (binding energy is 84.20 eV) or Au5Sn (binding energy is 84.14 eV), but it can not be distinguished from XPS because its resolution is about 0.3 eV. There is no peak shift before and after Ar ion beam sputtering, indicating a stability of Au chemical phase along with nanowire length. The Sn 3d 5/2 spectra consist of two peaks located at 484.3 eV and 486.4 eV (marked by two double white lines), indicating a formation of metallic Sn and SnOx respectively. This result indicates that the top ends of the 1D $Au_{80}Sn_{20}$ alloy solders which are exposed to air have been partly oxidized. After sputtering 240 s, the quantitative analysis of XPS wide spectrum reveals that the 1D $Au_{80}Sn_{20}$ nanosolders reach a stable 80.17:19.83 mass ratio of Au:Sn, and have not been detected any oxygen peak. Therefore, the chemical composition of the 1D $Au_{80}Sn_{20}$ nanosolders in this work is inferred to be $Au_{80}Sn_{20}$.

3.2. Welding individual TiO_2 nanowires together by using 1D $Au_{80}Sn_{20}$ nanosolders in situ TEM.

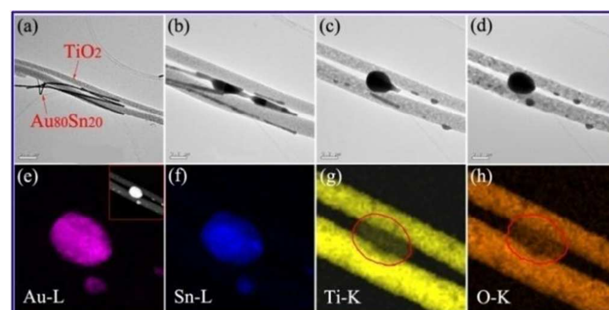

Fig. 3. (a-d) The welding process of two individual TiO_2 nanowires by using $Au_{80}Sn_{20}$ nanosolders in HRTEM. Bar = 0.2 µm. (e-h) EDX elemental mappings of Au-Lα (9.71 keV), Sn-Lα (3.44 keV), Ti-Kα (4.51 keV) and O-Kα (0.52 keV). Inset, the HADDF-STEM image of welded area.

Individual 1D $Au_{80}Sn_{20}$ nanosolders have been used in the application of welding nanopatterns at the nanoscale to test their quality as nanosolder. Fig. 3 shows the whole process of welding two TiO_2 nanowires together by using four 1D $Au_{80}Sn_{20}$ nanosolders via a high-energy electron beam irradiation nanowelding technique in situ HRTEM. The crossed structure (Fig. 3a) was achieved by successively dispersing the electrospun TiO_2 nanowires (see supplementary Fig. S4 for their structural and chemical characterization) and the 1D $Au_{80}Sn_{20}$ nanosolders on the holey carbon coated Cu grids. After the electron beam irradiated, the 1D $Au_{80}Sn_{20}$ nanosolders gradually melted (Fig. 3b), diffused into TiO_2 nanowires (Fig. 3c) and eventually welded the two TiO_2 nanowires together (Fig. 3d). The TiO_2 nanowires always remained their morphologies and structure during the whole welding process, which is due to their high melting point (the melting point of bulk TiO_2 is approximately 1800 ℃). However, Fig. 3d only intuitively displays a connection of the two TiO_2 nanowires. Solid evidence is required.

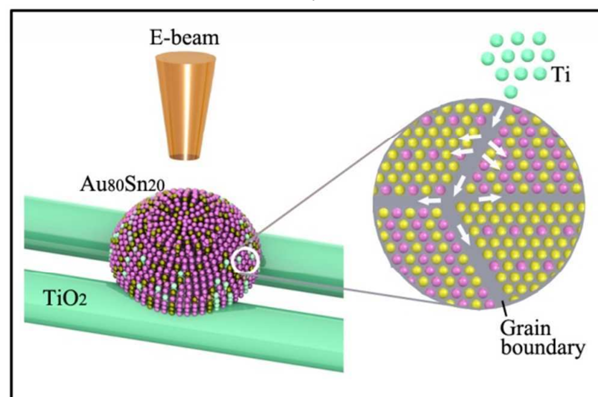

Fig. 4. Diagrams of the diffusion of Ti into $Au_{80}Sn_{20}$ nanosolder by grain boundaries diffusion mechanisms.

EDX elemental mapping technique was employed to check the quality of nanoweld. The inset of Fig. 3e shows a HADDF-

This journal is © The Royal Society of Chemistry 20xx

Journal of Materials Chemistry C Accepted Manuscript

STEM image of the welded junction, where the large white spot indicates a rich accumulation of gold and uniform chemical phase. Fig. 3e to 3h show the corresponding EDX elemental mappings of Au-Lα (9.71 keV), Sn-Lα (3.44 keV), Ti-Kα (4.51 keV) and O-Kα (0.52 keV), respectively. The elements of Au and Sn are evenly distributed throughout the welded junction, indicating the even $Au_{80}Sn_{20}$ chemical phase preserves after the welding and consistent with the HADDF-STEM observation. The elements of Ti and oxygen are also distributed throughout the welded junction. As the Sn is easy to be oxidized, it is deduced that the oxygen element of the welded junction mainly comes from the tin oxidization during the welding process. The Ti mapping reveals that the Ti element has diffused into the nanosolder residue after the welding of electron beam irradiation. Grain boundaries diffusion mechanism[31, 32] is speculated to cause the Ti diffusion into the $Au_{80}Sn_{20}$ nanosolder residue. As measured by above HRTEM and SEAD in Fig. 1c-1f, the individual 1D $Au_{80}Sn_{20}$ nanosolders is polycrystal, which is beneficial to the diffusion of Ti atoms into the grain boundaries of Au-based alloys according to the previous reports.[23] During the irradiation of electron beam, the Ti atoms diffused from the surface of TiO_2 nanowires into the grain boundaries of $Au_{80}Sn_{20}$ nanosolder. Then Ti atoms eventually left it and continued their diffusion in the lattice regions adjacent to the boundary, which thus gave rise to a volume diffusion zone around the boundary. Fig. 4 principally illustrates the schematic diagrams of the diffusion process. The continuous distribution of Ti element ranging from the welding bodies TiO_2 nanowires to the welded junction indicates a formation of integrally reliable bonding, showing that the welded junction should be electrically conductive and mechanically strong. This result also proves that the prepared $Au_{80}Sn_{20}$ nanosolder in this work should be suitable in the applications of welding other titanium-based nanomaterials.

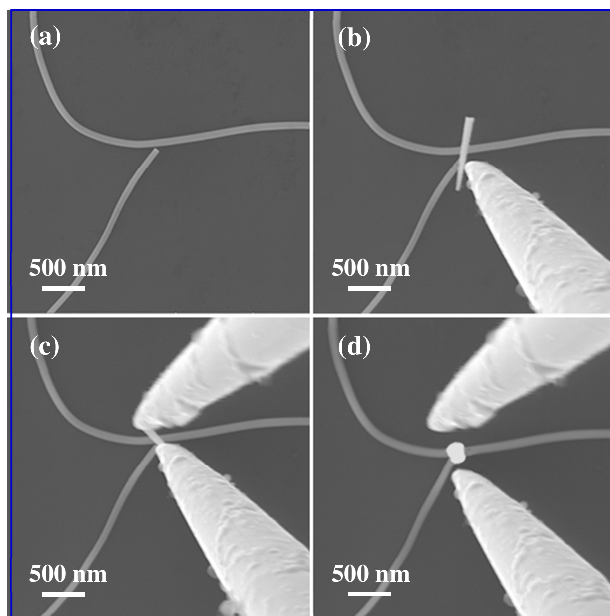

Fig. 5. Nanowelding two 110 nm TiO_2 nanowires using a sacrificial 1D $Au_{80}Sn_{20}$ nanosolder by nanomanipulators in situ SEM. (a) Assembly of a "人" nanopattern; (b) Placement of the sacrificial 1D nanosolder in contact with the nanostructure to be welded; (c) Preweld softening of the 1D nanosolder and contact to the two nanowires to be welded; (d) Nanowelding the nanowires together by a rectangular voltage pulse through the solder nanowire, causing significant material diffusion onto the junction.

The welding test was also performed by nanomanipulators in situ SEM. Figure 5 illustrates the whole proccess, which is the same as our previous reports.[9, 29] Two TiO_2 nanowires with 110 nm diameter were mechanically manipulated and assembled into a simple nano-pattern like Chinese word “人” on a SiO_2 (100nm)/Si wafer (Fig. 5a), and then a sacrificial 1D $Au_{80}Sn_{20}$ nanosolder with 130 nm diameter and 1.3 um length used as nanosolder was placed onto the assembled “人” nanopattern at the weld point as shown in Figure 5b. Prior to welding, a moderate current (about 80% maximum current density of a single 130 nm 1D $Au_{80}Sn_{20}$ nanosolder) was applied to soften the $Au_{80}Sn_{20}$ nanosolder for 1 ~ 2 minutes, which was for inducing the first join to the pattern (Fig. 5c). The softening of the sacrificial nanosolder is due to Joule-heating and can greatly improve the controllability and reliability of the nanowelding procedure. A linear pulse signal of 1.5 V and 300 ms width was then run through the solder to form the weld utterly. The short voltage pulse causes significant Joule heating and associated rapid material diffusion of the 1D nanosolder onto the chosen junction (Figure 5d). During the whole welding process, the 1D $Au_{80}Sn_{20}$ nanosolder showed a good mechanical strength, controllability, reliability and wettability with the TiO_2 semiconductor nanowires. The mechanical strength of the $Au_{80}Sn_{20}$ solder nanojoint was strong enough to enable welded structures to be directly lifted up by a SEM nanomanipulator. This result further proves that the 1D $Au_{80}Sn_{20}$ nanosolder is a reliable

Journal of Materials Chemistry C Accepted Manuscript

This journal is © The Royal Society of Chemistry 20xx

Please do not adjust margins

and high performance nanosolder material for welding titanium-based materials in the nanoscale space.

3.3. Infiltration experiment.

Infiltration experiment was further carried out to verify the solderability between TiO_2 nanowires and $Au_{80}Sn_{20}$ nanosolders. Fig. 6 shows the SEM images of individual 1D $Au_{80}Sn_{20}$ nanosolders after sintered by a tube furnace on TiO_2 substrate and SiO_2 substrate, revealing that the wire-shaped $Au_{80}Sn_{20}$ nanosolders have been melted into spherical particles (about 1 μm in diameter). The choice of SiO_2 substrate is only for a comparison. In order to observe the internal bonding features between the nanosolder particles and substrates, in-situ SEM nanomanipulators equipped with nichrome nanoprobes/nanotips were used to mechanically push away the formed nanosolder particles (Fig. 6a and 6d), which reveals whether there is inter-diffusion between the nanosolder and substrates. The contact angle was obtained by rotating sample stage to 90°, as shown in Fig. 6c and 6f. In the case of TiO_2 substrate, it is seen that the contact angle is smaller than 90°, revealing that the $Au_{80}Sn_{20}$ nanosolders well spread on the surface of TiO_2 substrate. This result proves that the $Au_{80}Sn_{20}$ nanosolders can infiltrate with TiO_2. In addition, it is also seen that the contrast of left mark is quite bright, revealing a large amount of $Au_{80}Sn_{20}$ nanosolder residue left. This result indicates that a solid connection between the TiO_2 and $Au_{80}Sn_{20}$ nanosolder was formed, which is consistent with above welding experiment as shown in Fig. 3 and Fig. 5.

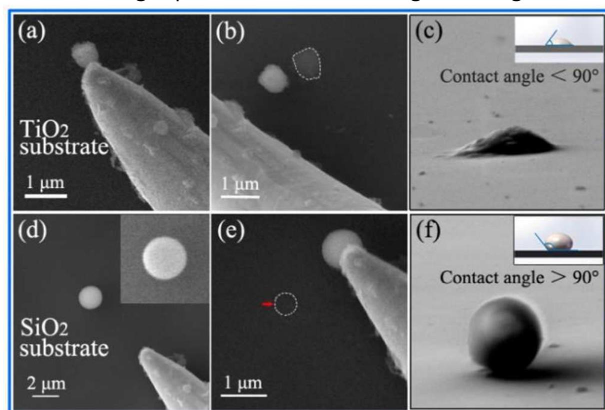

Fig. 6. The result of infiltration experiment for $Au_{80}Sn_{20}$ nanosolders with TiO_2 and SiO_2 substrates: (a) Nanoprobe approaching the sintered nanosolder on TiO_2 substrate. (b) The bonding trace left after the nanosolder was pushed away by the nanoprobe on TiO_2 substrate. (c) The lateral profile of a melted nanosolder on TiO_2 substrate. (d) Nanoprobe approaching the sintered nanosolder on SiO_2 substrate. (e) The non-bonding trace left after the nanosolder was pushed away by the nanoprobe on SiO_2 substrate. (f) The lateral profile of a melted nanosolder on SiO_2 substrate.

In comparison with the case of SiO_2 substrate (Fig. 6d - 6f), an opposite result is observed. After the melted $Au_{80}Sn_{20}$ nanosolder particle on the SiO_2 substrate was pushed away by the nichrome nanoprobe (Fig. 6e), the left trace is hard to be observed (the original position marked by red arrow). From Fig. 6f, it is seen that the contact angle is bigger than 90° and the $Au_{80}Sn_{20}$ nanosolders do not infiltrate with SiO_2. That is, SiO_2 is not solderable by the $Au_{80}Sn_{20}$ nanosolders. The result was also verified by the welding of SiO_2 nanowires using 1D $Au_{80}Sn_{20}$ nanosolders in TEM as shown in Fig. S5. In addition, it is also seen in Fig. 6d and 6f that the melted $Au_{80}Sn_{20}$ nanosolder has an ideal spherical shape, revealing that the surfacial oxidization of individual 1D $Au_{80}Sn_{20}$ nanosolders as observed above (Fig. 1c) nearly does not influence their solderability and wettability. The comparative infiltration experiments further prove that the 1D $Au_{80}Sn_{20}$ nanosolders have a good solderability and wettability to TiO_2 semiconductor.

4. Conclusions

In summary, we have demonstrated a fabrication of 1D $Au_{80}Sn_{20}$ nanosolders and applied them into the welding of individual TiO_2 semiconductor nanowires at the nano scale for the first time. The analysis of crystal structures prove that the individual $Au_{80}Sn_{20}$ alloy nanosolders contain two eutectic phases, including Au5Sn and AuSn phases. Chemical analysis confirm that the mass ratio of Au:Sn is 80:20. The experimental results also reveal that the Ti element has diffused into the nanosolder residue during the welding of electron beam irradiation, which is further confirmed by the infiltration experiments. The good solderability and wettability between the 1D $Au_{80}Sn_{20}$ nanosolders and TiO_2 materials indicate that the $Au_{80}Sn_{20}$ nanosolder should be also suitable in the applications of welding other titanium-based nanomaterials. Our work is believed to contribute a special nanosolder for future nanoindustry, which can realize the bonding of tin-based semiconductor oxide nanomateirals at the nanoscale.

Acknowledgements

This work is supported by National Basic Research Program of China (2012CB933104), National Natural Science Foundation of China (11274145 and 51571104), MOST International Cooperation Funds (2014DFA91340), Program for Changjiang Scholars and Innovative Research Team in University (Grant No. IRT1251), and the Fundamental Research Funds for the Central Universities (lzujbky-2013-19, and 2022013zrct01).

Notes and references

1 A. Figuerola, I. R. Franchini, A. Fiore, R. Mastria, A. Falqui, G. Bertoni, S. Bals, G. V. Tendeloo, S. Kudera, R. Cingolani and L. Manna, *Adv. Mater.,* 2009, **21**, 550-554.
2 Y. N. Xia, P. D. Yang, Y. G. Sun, Y. Y. Wu, B. Mayers, B. Gates, Y. D. Yin, F. Kim and Y. Q. Yan, *Adv. Mater.,* 2003, **15**, 353-389.
3 S. Han, S. Hong, J. Ham, J. Yeo, J. Lee, B. Kang, P. Lee, J. Kwon, S. S. Lee, M. Y. Yang and S. H. Ko, *Adv. Mater.,* 2014, **26**, 5808-5814.
4 Y. Wu and P. Yang, *Adv. Mater.*, 2001, **13**, 520-523.

This journal is © The Royal Society of Chemistry 20xx

Journal of Materials Chemistry C Accepted Manuscript

5 Z. Wang, L. Yu, W. Zhang, Y. Ding, Y. Li, J. Han, Z. Zhu, H. Xu, G. He, Y. Chen and G. Hu, *Phys. Lett. A*, 2004, **324(4)**, 321-325.
6 V. Gopal, V. R. Radmilovic, C. Daraio, S. Jin, P. Yang and E. A. Stach, *Nano Lett.*, 2004, **4(11)**, 2059-2063.
7 J. K. Seol and J. D. Jeon, App. Phys. Lett., 2005, **86 (3)**, 033112.
8 C. Chen, L. Yan, E. Kong and Y. Zhang, *Nanotechnology*, 2006, **17**, 2192-2197.
9 Y. Peng, A. G. Cullis and B. J. Inkson, *Nano Lett.*, 2009, **9**, 91-96.
10 S. Xu, M. Tian, J. Wang, J. Xu, J. M. Redwing and M. H. W. Chan, *Small*, 2005, **1(12)**, 1221-1229.
11 H. Tohmyoh, T. Imaizumi, H. Hayashi and M. Saka, *Scripta Mater.*, 2007, **57(10)**, 953-956.
12 H. Tohmyoh, *J. Appl. Phys*., 2009, **105**, 014907.
13 H. Hirayama, Y. Kawamoto, Y. Ohshima and K. Takayanagi, *Appl. Phys. Lett*., 2001, **79(8)**, 1169-1171.
14 D. N. Madsen, K. Mølhave, R. Mateiu, A. M. Rasmussen, M. Brorson, C. J. H. Jacobsen and P. Bøggild, *Nano Lett.,* 2003, **3**, 47-49.
15 J. H. Ahn, H. S. Kim, K. J. Lee, S. Jeon, S. J. Kang, Y. G. Sun, R. G. Nuzzo and J. A. Rogers, *Science*, 2006, **314**, 1745-1757.
16 L. D. Zhang and X. S. Fang, *J. Nanosci. Nanotechnol*. 2008, **8(1)**, 149-201.
17 P. Ravirajan, D. D. C. Bradley, J. Nelson, S. A. Haque, J. R. Durrant, H. J. P. Smit and J. M. Kroon, *Appl. Phys.Lett.*, 2005, **86**, 143101.
18 A. Kitiyanan and S. Yoshikawa, *Mater. Lett*., 2005, **59**, 4038-4040.
19 R. H. Wang, C. M. Ruan, D. Kanayeva, K. Lassiter and Y. B. Li, *Nano Lett*., 2008, **8**, 2625-2631.
20 Z. Jin, *patent*, **CN 201310571335**, 2014.
21 J. M. Poate, P. A. Turner and W. J. DeBonte, *J. Appl. Phys*., 1975, **46**, 4275-4283.
22 E. M. William, G. Giuliano and M. Thomas, *Thin Solid Films*, 2010, **518**, 2585-2591.
23 D. Kim and C. C. Lee, *Mater. Sci. Eng. A*, 2005, **416**, 74-79.
24 V. Chidambaram, J. Hattel and J. Hald, *Mater. Des.*, 2010, **31**, 4638.
25 J. H. Kuang, M. T. Sheen, C. H. Chang, C. C. Chen, G. L. Wang and W. H. Cheng, *IEEE Trans. Adv. Packag*., 2001, **24**, 563.
26 G. Elger, M. Hutter, H. Oppermann, R. Aschenbrenner, H. Reichl and E. Jager, *Microsyst. Technol*., 2002, **7**, 239.
27 J. W. R. Tew, X. Q. Shi and S. Yuan, *Mater. Lett*., 2004, **58**, 2695.
28 Y. Peng, H. L. Zhang, S. L. Pan and H. L. Li, *J. Appl. Phys*., 2000, **87**, 7405.
29 H. Zhang, J. W. Zhang, Q. Q. Lan, H. B. Ma, K. Qu, B. J. Inkson, N. J. Mellors, D. S. Xue and Y. Peng, *Nanotechnology*, 2014, **25**, 425301.
30 X. D. Li, C. T. Gao, H. G. Duan, B. A. L, X. J. Pan and E. Q. Xie, *Nano Energy*, 2012, **1**, 640-645.
31 A. E. Austin and N. A. Richard, *J. Appl. Phys*. 1961, **32**, 1462-1471.
32 C. Herzig and S. V. Divinski, *Mater. Trans*., 2003, **44**, 14-27.

Journal of Materials Chemistry C Accepted Manuscript

This journal is © The Royal Society of Chemistry 20xx

Please do not adjust margins